ELSEVIER

Journal of Nuclear Materials 266–269 (1999) 189–196

journal of nuclear materials

Comparison of ergodic and axisymmetric divertors

Ph. Ghendrih *, A. Grosman, J. Gunn, F. Laugier, B. Meslin, C. Grisolia, R. Guirlet, P. Monier-Garbet, T. Loarer

Association Euratom-CEA, DRFC, CEA Cadarache, 13108 St Paul lez Durance, Cedex, France

Abstract

Ergodic and axisymmetric divertor configurations are shown to follow identical physics insofar as parallel transport is a dominant feature. As a consequence a unique 1-D model is used to model the divertor density regimes. This model indicates qualitatively that impurity radiation will lower the threshold to detachment and that the Mach number exhibits a maximum close to the ionization front. Experimental data corresponding to the density regimes, thermal bifurcation on a given flux tube and Mach number profile illustrate the behaviour of the divertor states. It is shown that closed divertors should exhibit sharp transitions to detachment, as reported on DIII–D, while open divertors are characterized by a gradual detachment. Evidence of this behaviour is given for Tore Supra. Discussion of the relationship between the upstream SOL density of the model and the volume average density are discussed in the frame of a comparison between open and closed divertors. Depending on the tightness of the divertor with respect to neutral recirculation, it is shown that the effective control parameter, volume average density or gas injection, will change.

Keywords: Detachment; Divertor physics; Ergodic divertor; 1-D model

1. Introduction

Significant progress towards high performance plasmas in fusion devices has been achieved by implementing specific components dedicated to plasma–wall interaction. The step from passive extraction components to axisymmetric (or poloidal) divertors has opened the way to controlled edge plasma transport and outstanding results on confinement, impurity screening and power deposition [1]. These results, the number of devices operating with the axisymmetric divertor, and the level of understanding exemplified by the sophisticated numerical modelling [2], have governed the choice of this divertor for the ITER project. The very goals of the latter project have led to a renewal in the interest in divertor physics [3]. Indeed, the time scale of the foreseen experiments, typically 1000 s, impose steady operation of the heat extraction components and therefore technological limitations in the energy flux [4]. Compatibility between energy deconfinement in the divertor volume and high core confinement have led to decoupling core and divertor volumes by mechanical baffling of the neutrals [5]. The tightness of such closed divertors with respect to particle recirculation is weakened by spurious recycling on the baffles during ELMs or on the ICRH and LH antennae in regimes of sufficient plasma–wave coupling. The ergodic divertor, still on operation on Tore Supra, can appear as an alternative divertor [6]. In the present paper, the comparison between these divertors is focused on the issue of mechanical closure versus open divertor operation. Indeed, the closure of the ergodic divertor volume is ensured by the plasma itself, and the issue of tightness is then raised in high density operation as the screening capability weakens. In Section 2, the principle and geometrical properties of the two divertor configurations are recalled. Plasma edge density scaling versus the volume averaged density is presented in Section 3. Section 4 is devoted to the overall particle recirculation and its impact on the location of the ionization front. Results are discussed in Section 5.

* Corresponding author.

0022-3115/99/$ – see front matter
PII: S0022-3115(98)00525-X

2. Divertor geometry and operational window

The very first aim of divertors is to remove the region devoted to plasma wall interaction from the last closed flux surface which we call separatrix for convenience. This change of topology is governed by external magnetic fields and thus specific set of divertor coils. In the case of the axisymmetric divertor a singular point with vanishing poloidal magnetic field (X-point) is generated by an $n=0$, $m=1$ coil sustaining a current comparable to the plasma current. The target plates are located on the 'legs' below the X-point with respect to the core plasma. The singularity generates a logarithmic divergence in the field line connexion lengths and a specific volume dedicated to divertor physics from the X-point to the target plates. In the case of the ergodic divertor a resonant magnetic perturbation is used to generate singularities in the magnetic field topology. On Tore Supra the coil system generates an $n=6$, $m=18\pm6$ perturbation [6]. This external perturbation will destroy the magnetic surfaces at the plasma boundary, typically $\rho\geqslant 0.8$ ($\rho=r/a$, a being the plasma minor radius), and above a threshold in the perturbation current. The operational window is restricted to values of the plasma current such that the main modes of the perturbation are resonant at the plasma boundary, hence $q(r=a)\sim(18\pm6)/6$.

Given the interplay between charged particles and neutral particles in the plasma boundary, the relevant geometry is governed by two different metrics. On the one hand, neutral transport is governed by atomic physics scales, namely the ionization and charge exchange mean free paths, λ_{I} and λ_{CX} respectively. As a result the typical scale strongly depends on the line integrated plasma density over the neutral line of flight.

$$1=\int_0^{\lambda_{\mathrm{I}}} \mathrm{d}\zeta \frac{n\langle\sigma v\rangle_{\mathrm{I}}}{v_0}. \tag{1}$$

In this definition one recognises the ionization rate $\langle\sigma v\rangle_{\mathrm{I}}$, the plasma density n, the neutral velocity v_0 and the abscissa along the line of flight, $\varsigma=\rightarrow\varsigma_{.0}/v_0$. On the other hand, the plasma scale depends on strongly magnetized plasma transport properties. Provided transport parallel to the magnetic field is the largest, the equilibrium magnetic fluxes then define the proper metric and the transport radial step in real space is proportional to the flux expansion. Typical scales, such as the density e-folding length $\lambda_{\mathrm{n}}=(D_\perp L_{//}/c_{\mathrm{S}})^{1/2}$, are mapped to the midplane. This scale depends on the particle diffusivity $D_\perp$ (provided this is the proper transport process [7]), on parallel transport at sound velocity c_{S}, and on the relevant parallel scale $L_{//}$. Energy transport impacts particle recirculation through the temperature dependence of the ionization rate, the sound velocity and neutral velocity. Geometrical control of particle recirculation is therefore achieved via the launching point of recycling neutrals (where $\varsigma=0$), the wall to separatrix radial distance δ_{div}, and the parallel scale $L_{//}$. This geometrical control is only effective insofar that plasma–neutral interaction is significant. The wall to separatrix distance δ_{div} thus exhibits large poloidal variations in the axisymmetric divertor. Neutral influx must therefore be maintained in the vicinity of the X-point where δ_{div} is maximum. Poloidal symmetry of δ_{div} in the case of the ergodic divertor configuration is thus compatible with a distributed neutral source around the torus with no mechanical baffling. The impact of the parallel scale is more difficult to analyse. The connexion length diverges from the wall to the separatrix in both configurations. Results for the ergodic divertor are characterized by a large region of long connexion lengths, with significant modulations radially and poloidally. It could be argued that the feature alone would lead to large density e-folding lengths. However, transport analysis indicates that plasma properties only depend on $L_{//}$ up to a limit in the range of πqR, the standard limiter connexion length [6,8].

3. Density regimes

Characterization of divertor performance is achieved by analyzing the divertor density response to either a core density or a gas injection scan. Three regimes are routinely reported with the axisymmetric divertor [1,9] and have been recovered with the ergodic divertor [10], Fig. 1. At low density a linear dependence of the divertor density, n_{div}, versus the volume averaged density $\langle n_{\mathrm{e}}\rangle$ is observed. The high recycling regime is then found once a critical temperature is reached. Following a standard analysis [1], this regime follows the scaling $n_{\mathrm{div}}\propto\langle n_{\mathrm{e}}\rangle^3$. Finally detachment occurs, namely a roll-over of the divertor density or more precisely a drop of n_{div} below the $\langle n_{\mathrm{e}}\rangle^3$ scaling followed by a decrease of n_{div} as $\langle n_{\mathrm{e}}\rangle$ is further increased. Let us consider a 1-D model of plasma parallel transport to the target plates. Such a model should capture the basic features of the involved physics as long as transverse transport can be neglected, typically for a connexion length bounded to $L_{//}=\pi qR$ (the laminar regime in the ergodic divertor configuration [6]). At the present stage, the model is used as a qualitative guideline to analyze the experiments. The linear regime allows one to determine the power influx and a crude model is used for the impurities. For the attached regime, the mechanical balance leads to a regime at constant pressure $\Pi=2nT(1+M^2)$, T is the temperature for this single fluid approach ($T_{\mathrm{e}}=T_{\mathrm{i}}$) and M is the Mach number. It is also assumed that the conductive flux is much larger than the convective flux, this very assumption being in fact the definition of the attached regime. Control parameters are Q_{up} the upstream energy influx into the given flux line and n_{up} the upstream

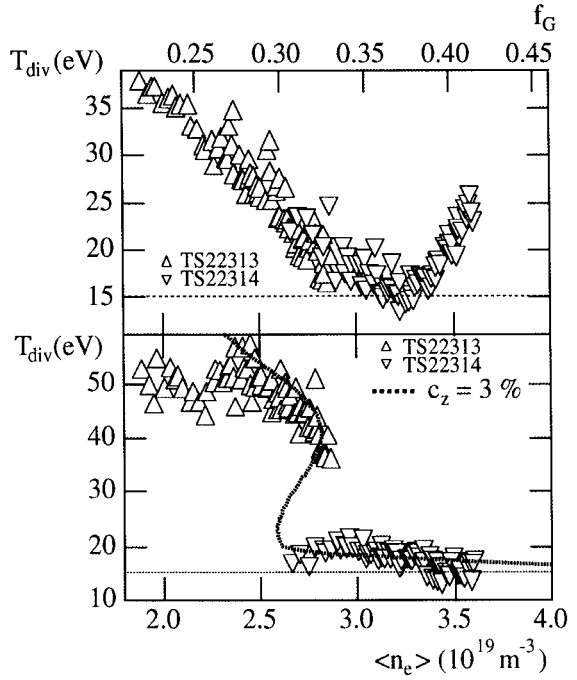

Fig. 1. Experimental evidence of the divertor density regimes achieved with the ergodic divertor when the volume averaged density is increased. Top, divertor density, linear regime up to $f_G \sim 28\%$ of Greenwald density and detachment at $f_G \sim 33\%$. Stable detached regime in this ohmic operation is achieved up to $f_G \sim 41\%$. Lower, divertor temperature data and 1-D model results. The experiment was performed with a mixed gas injection, deuterium and nitrogen, to enforce a constant impurity content.

density. Given the strong temperature dependence of the ionization cross section and of the parallel heat conductivity, $\kappa_{//} = \bar{\kappa}\, T^{5/2}$, one finds two characteristic temperatures, $T_{\Delta} \sim 10$ eV below which the ionization rate decreases rapidly and $T_{//}$ which is the minimum upstream temperature with no energy loss along the field line.

$$T_{//} = \left[\left(Q_{\rm up} L_{//} \right) \Big/ \left(\frac{2}{7} \bar{\kappa} \right) \right]^{2/7}. \tag{2}$$

In this equation $Q_{\rm up} \sim q$ (q is the conducted energy flux) as would be expected for a large temperature low particle flux regime. At constant energy flux along the field line the temperature equation is readily integrated and yields $T(s) = T_{//}[(s/L_{//}) + (T_{\rm div}/T_{//})^{7/2}]^{2/7}$. $T_{\rm div}$, the plasma temperature at the target plate appears therefore as a key parameter. Given the Bohm sheath conditions, one finds that this temperature is defined as $T_{\rm div} = Q_{\rm div}/(\gamma \Gamma_{\rm div})$, $Q_{\rm div}$ and $\Gamma_{\rm div}$ being respectively the parallel energy and particle flux to the target plate. The sheath transmission factor is $\gamma \sim 6$. The large particle flux which characterizes divertor operation thus governs low divertor temperatures. At low fuelling efficiency, any density increase will thus induce a further lowering of the divertor temperature. Particle recirculation is therefore the key feature of divertor operation. Another effective means of lowering $T_{\rm div}$ is the reduction of $Q_{\rm div}$ due to impurity line radiation [11]. At low density, and therefore at high divertor temperature, impurity radiation is small so that one finds $T_{\rm div} \geqslant T_{//} (T_{//} \sim 30$ to 40 eV in ohmic shots). The parallel temperature gradient is small so that upstream ($n_{\rm up}$) density is a factor 2 larger than the divertor density, $n_{\rm div}$. The transition from linear to high recycling regimes thus occurs when $T_{\rm div} \sim T_{//}$. Below this temperature, another feature modifies the behaviour of the divertor parameters, namely impurity radiation. In the following equation, the temperature profile is defined following the calculation of Ref. [12]. Impurity radiation is introduced via a given impurity concentration c_z and the radiation rate $L_z(t)$. It is assumed that c_z is constant, of the order of 3%, and unless specified independent of $T_{\rm div}$.

$$T_{//}^{7/2} = \frac{7}{2} \int_{T_{\rm div}}^{T_{\rm up}} \frac{T^{5/2} {\rm d}T}{\left(1 - \frac{\Pi^2}{2 Q_{\rm up}^2} c_z W(T) \right)^{1/2}};$$

$$W(T) = \int_{T}^{T_{\rm up}} \frac{\kappa_{//} L_z(T) {\rm d}T}{T^2}. \tag{3}$$

Radiation is assumed to occur at low Mach number so that density is expressed in terms of the temperature and the constant pressure Π.

$$\Pi = 2 n_{\rm up} T_{\rm up} = 2 n_{\rm div} T_{\rm div} (1 + M_{\rm div}^2). \tag{4}$$

In the attached regime it is possible to relate the pressure to the energy and particle flux at the sheath boundary so that the pressure is defined for a given upstream energy flux.

$$\frac{\Pi}{Q_{\rm up}} = \left\{ \frac{\gamma^2 M_{\rm div}^2}{2 \left(1 + M_{\rm div}^2 \right)^2} \frac{T_{\rm div}}{m_{\rm i}} + \frac{c_z}{2} W(T_{\rm div}) \right\}^{-1/2}. \tag{5}$$

This expression clearly shows that the impurity radiation, typically $c_z\, W(T_{\rm div})$ in Eq. (5), lowers the available plasma pressure Π at given injected power. However this effect must be larger than the sheath energy convection (other term on the RHS of Eq. (5)) to induce strong effects. In practice, one finds that intrinsic impurity radiation becomes significant for temperatures lower than ~ 40 eV. The transition from linear to high recycling induces in fact a transition into the radiating divertor regime. For sufficiently peaked radiation rates, multiple steady state solutions are found [12], with two branches such that ${\rm d}n_{\rm div}/{\rm d}n_{\rm up} \geqslant 0$, Fig. 2. One also finds that the divertor density increase versus the upstream density is much sharper than the cubic scaling which corresponds to the experimental regime of Fig. 1. It

must also be underlined that bifurcation points are associated to infinitely long relaxation processes to equilibrium. As a consequence, density ramps can depart from adiabatic variations of the control parameter, and the measured data correspond to transient states with little relevance to equilibrium states, see Ref. [13]. This might explain why there is no clear evidence of a bifurcation in the experimental data displayed on Fig. 1. Finally, since impurity line radiation is still large in the 10 eV range, one finds that the radiating divertor regime (the high recycling regime) leads to the detached regime after only a minor increase of the upstream density. This is also readily observed in the experimental data of Fig. 1, with the roll-over of the density increase at $\langle n_e \rangle \sim 3 \times 10^{19}$ m^{-3}, typically 35% of the Greenwald density. Using the JET definition of the degree of detachment (DoD) [14], one can associate to this roll-over, a progressive increase of the divertor detachment related to a pressure drop along the field lines [14]. On Tore Supra, the increase of the DoD is shown to be related to a shift of the radiation front [15,16], a feature also reported in axisymmetric divertor experiments such as JT60-U [17], DIII–D [18] and C-Mod [19]. Bifurcation like behaviour of the divertor parameters has been observed in a specific set of experiments with a very low level of intrinsic impurities dominated by carbon. As the volume averaged density is increased, one observes an exponential decrease of the carbon content of the discharge which one readily interprets in terms of a lowered sputtered yield as the divertor temperature is lowered. Similar behaviours are found in helium plasmas where the density can be increased up to the Greenwald density with no detachment the temperature remaining above 10 eV and the carbon content decreasing steadily. This behaviour with no pressure drop along the field lines is also reported for DIII–D helium operation [20]. This variation of the impurity concentration is equivalent to a strong decrease of the radiation rate as T_{div} approaches 10 eV. This sharpens the radiation peak but also allows the plasma to remain in the attached regime at a larger volume averaged density. In the sequence of two shots with different density ranges, one observes that the high temperature branch followed by the low temperature branch is measured at one location of the target plates, Fig. 3. Matching of the temperatures is observed at another location, the steady decrease of T_{div} being followed by an increase of T_{div} as the volume averaged density is further increased, Fig. 3. The latter behaviour is reported in the C-Mod divertor experiments, the so called 'death ray' effect [9]. Modelling of the coupled effect of impurity radiation and decay of the impurity source allows one to recover qualitatively the behaviour of the bifurcated regime and in particular the clamping of T_{div} to the 15 eV range despite the increase of both n_{div} and n_{up}, Fig. 3. The 'death ray' regime cannot be analysed in terms of the 1-D model, since it appears to be related to a specific increase of the energy flux on several flux tubes as the density is increased so that the divertor plasma appears to reattach, T_{div} increases and n_{div} decreases. Similarly to C-Mod observations, the death ray is observed prior to detachment which is not reached in this low impurity content plasma up to 41% of the Greenwald density.

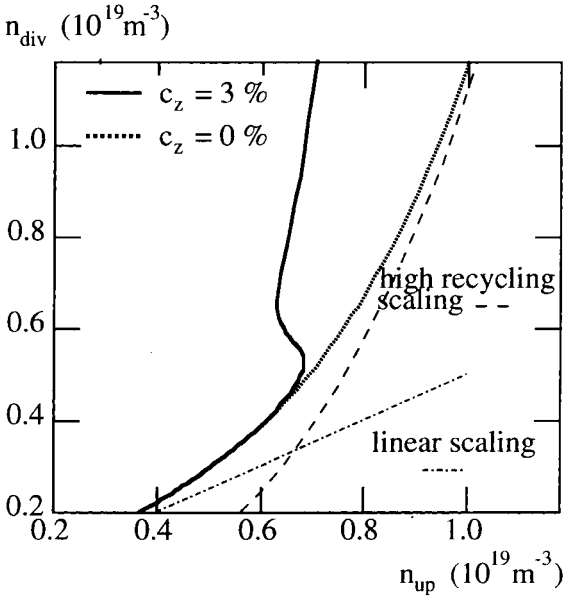

Fig. 2. 1-D model result for the divertor density against the upstream density, results for the divertor temperature with the same parameters are plotted on Fig. 1. Impurity radiation induce a bifurcation of the divertor plasma state with very long relaxation times (at the bifurcation points) and unstable equilibrium states. Note that the divertor density departs from the linear scaling before the transition point even with no impurity.

4. Particle recirculation and location of the ionization front

Modelling the detached regime requires to properly account for the coupling between mechanical and particle balance:

$$\frac{d\Gamma}{ds} = n n_N \langle \sigma v \rangle_I \approx n_N \frac{\langle \sigma v \rangle_I}{T}(nT);$$
$$\frac{d\Pi}{ds} = -m_i n_N \langle \sigma v \rangle_{CX} \Gamma. \quad (6)$$

At large increase of the particle flux Γ along the magnetic field (curvilinear abscissa s) quenches the conductive energy flux inducing the strong reduction in the temperature gradient required for the detached regime. The rapid variation of the right-hand side of the balance equations governs significant changes in the Mach

number. Let us introduce $\mathscr{M} = (2|M|)/(1+M^2)$ such that:

$$\mathscr{M} = \frac{4T|\Gamma|}{\Pi c_S}; \quad \frac{d\mathscr{M}}{\mathscr{M} ds} = \frac{1}{2L_{CX}} \left\{ \frac{L_{CX}}{T} \frac{dT}{ds} - \left(\mathscr{M} + \frac{2\langle\sigma v\rangle_I}{\langle\sigma\rangle_{CX}} \frac{1}{|M|} \right) \right\} \quad (7)$$

The scale L_{CX} is the charge exchange mean free path $L_{CX} = c_S/(n_N\langle\sigma v\rangle_{CX})$ where c_s is the sound velocity $c_S = (2T/m_i)^{1/2}$. Two sets of terms govern the parallel variation of the Mach number, the positive temperature gradient induces a reduction of the Mach number as one approaches the target plates while the parallel pressure drop towards the target plate and the particle flux increase to the target plate generate the standard increase of the Mach number towards the target plate. The sequence of changes of the dominant processes governs the modification in Mach number parallel profile. As s decreases towards the target plate, one observes a first regime at low Mach number where ionization is the dominant process in the variation of the Mach number, the Mach number follows the standard behaviour [21], Fig. 4. In the vicinity of the ionization front, the temperature gradient becomes very large and the ionization process is strongly reduced as $T_{div} \leqslant 10$ eV. The Mach number then decreases until the reduction of the temperature gradient in the detached plasma allows for a Mach number increase to the target plate driven by the parallel momentum loss, Fig. 4. Neglecting variations of the energy flux, one can relate the location of the maximum of the Mach number Δ_M to the location of the ionization front Δ which also labels the detachment front [22,23].

$$\Delta_M = \Delta + \frac{2L_{CX}}{7\left(\mathscr{M} + \frac{2\langle\sigma v\rangle_I}{\langle\sigma v\rangle_{CX}} \frac{1}{|M|}\right)}. \quad (8)$$

One thus finds that the front of the Mach number maximum stands just ahead of the ionization front, $L_{CX}/L_{//} \sim 0.04$ with $n_N \sim 4 \times 10^{18}$ m^{-3}, Fig. 4. While

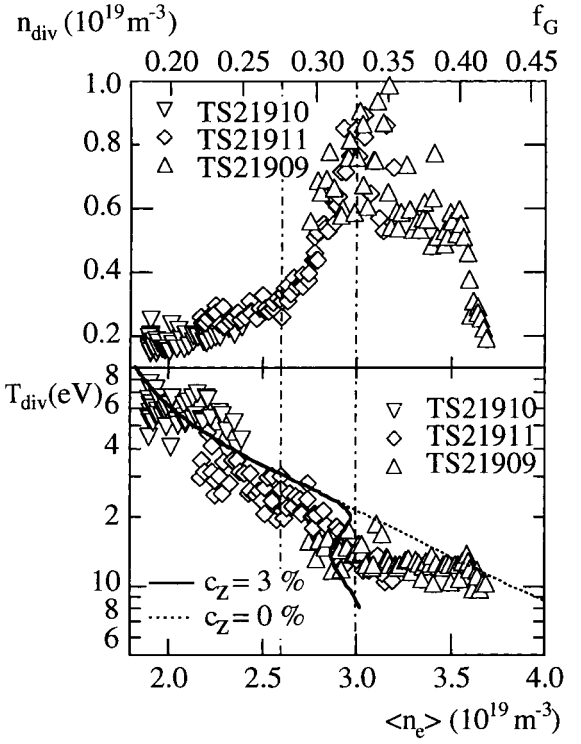

Fig. 3. Experimental data of the divertor temperature for two Langmuir probes at different locations toroidally and poloidally. The top graph with data from a midplane probe (field line leaving the probe in the counter direction) is characterized by a smooth decrease of the temperature followed by a shoot up near the detachment limit, a behaviour which is reminiscent of the C-Mod 'death ray'. On the lower graph, data is taken from a probe slightly above midplane from an adjacent module for a field leaving the probe in the co direction. The strong bifurcation behaviour is recovered with the 1-D model by introducing a strong lowering of the impurity content below 20 eV. The strong decrease of the intrinsic impurities (carbon and oxygen) is also reported experimentally as the volume averaged density is increased.

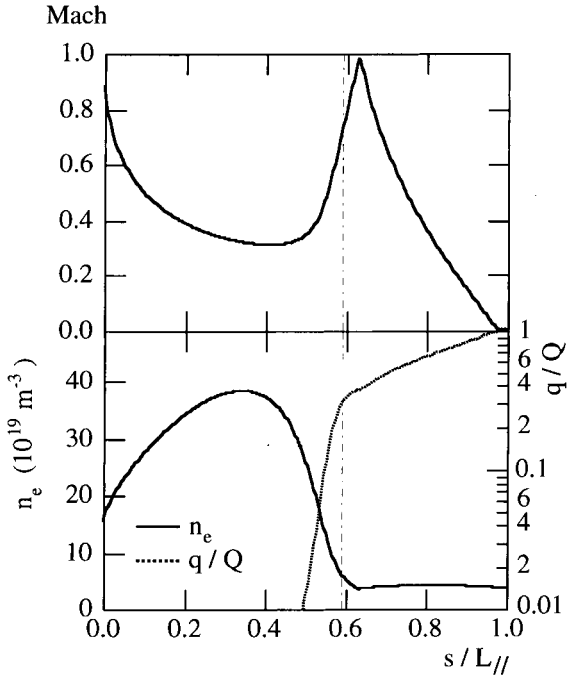

Fig. 4. 1-D analysis of the Mach number profile along a field line from the wall $s = 0$ and $M = 1$. The density profile and the ratio of the conductive energy flux q over the total energy flux Q are plotted on the lower graph. Detachment, characterized by the sharp decrease of the ratio q/Q is shown to occur in the very vicinity of the local maximum of the Mach number.

such a measurement is impossible in the axisymmetric divertor configuration, the ergodic divertor offers a unique opportunity since the radial scan of the reciprocating probe is equivalent to a parallel scan along the field line, Fig. 5. Although the exact matching between the radial location and the parallel connexion length is difficult to unfold, the measurement of the Mach number [24,25] displays a marked maximum at $|M| \sim 1$ inside the plasma when detachment occurs, Fig. 5. The measurement thus allows one to monitor the inward shift of the ionization front as the volume averaged density is increased. The relationship between the maximum of the Mach number and the ionization front is reinforced by the measured temperature near the maximum of $|M|$, $T_e \sim 10$ eV (sudden drop in T_e at $r = 0.75$ m), Fig. 5. The gradual inwards radial shift of the ionization front is equivalent to a progressive shift of the ionization front along the field line, Fig. 6. This agrees with the notion of a degree of detachment [14] which differs strongly from the bifurcation like phenomena reported for DIII–D [26]. In the latter experiment, the sudden changes of the divertor behaviour [27], at critical neutral pressure in the private flux region [26] is interpreted as a sudden change in the location of the ionization front [22]. This striking difference in behaviour appears to originate from two schemes of particle recirculation control. The analysis of the DIII–D detachment emphasizes the existence of a controlled neutral population which builds up in the private flux region

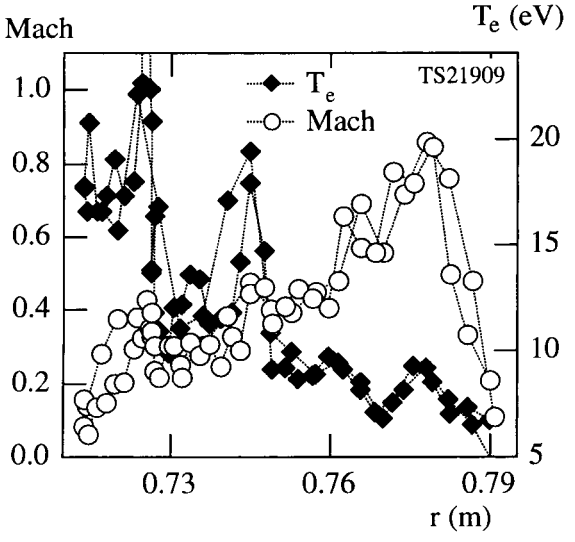

Fig. 5. Radial profile of the Mach number and of the temperature field obtained with the reciprocation Langmuir probe. In the ergodic divertor configuration such a radial scan also corresponds to a scan in the connexion length to the target plates. Note the relative stability of the divertor state highlighted by the similar profiles obtained during the back and forth movement of the probe.

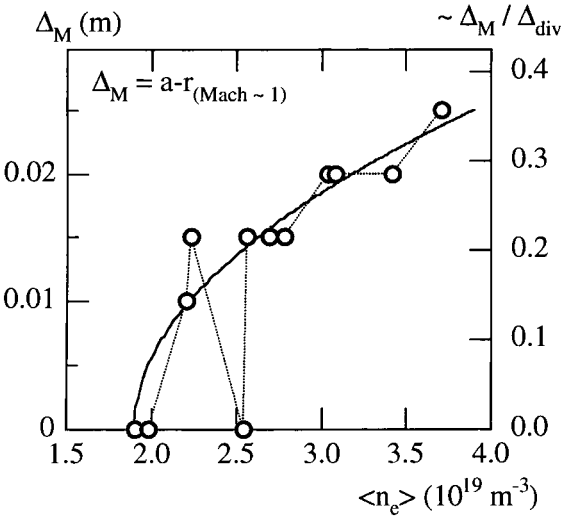

Fig. 6. Radial inward displacement of the $M \sim 1$ front Δ_M as the volume averaged density is increased. Right-hand side scale, ratio of Δ_M to Δ_{div} where Δ_{div} is the estimated extent of the low particle confinement region.

with no leakage out of the divertor volume. Furthermore, this experiment is characterized by strong neutral beam fuelling and no feedback control of the core density [27]. Integration of Eq. (6), in the attached region (Π = constant and $|M| \ll 1$) and in the detached region (Π decreases and $|\Gamma|$ = constant) at constant neutral density yields the location of the ionization front which is characteristic of the balance between the particle flux build-up and the pressure drop over a fixed total parallel extent of the field line L_N where neutrals are present [22].

$$\frac{(L_N - \Delta)\Delta}{L^{\Delta}_{CX} L^{\Delta}_{I}} + \frac{(L_N - \Delta)}{L^{\Delta}_{I}} - 1 = 0, \tag{9}$$

where the ionization and charge exchange mean free path are computed at the ionization front between the attached and detached region at $T_\Delta \sim 10$ eV, $L^{\Delta}_{I} = C^{\Delta}_{S} / (n_N \langle \sigma v \rangle^{\Delta}_{I})$, $L^{\Delta}_{CX} = C^{\Delta}_{S} / (n_N \langle \sigma v \rangle^{\Delta}_{CX})$ with $C^{\Delta}_{S} = (2T_\Delta / m_i)^{1/2}$. Replacing T_{div} by T and M_{div} by $M \sim 1$ in Eq. (5) yields $\Pi_\Delta = 2 n_{up} T_{up}$, which only depends on the upstream energy flux and on the radiated power in the radiating region. Beyond the radiating regime the energy flux is constant so that $T_{up} = T_{//} (1 - \Delta_R / L_{//})^{2/7}$, where Δ_R is the boundary of the radiating front. Assuming that the radiating region is not affected by the detached region, hence $\Delta_R - \Delta$ is constant, one finds that T_{up} and n_{up} are monitored by Δ provided that $\Delta / L_{//}$ is not too small. This analysis thus indicates that in a divertor configuration with low neutral control, hence $L_N \sim L_{//}$, the feedback control of n_{up} allows one to control Δ and the required neutral density to achieve n_{up}. This scheme does not yield bifurcations although a large variation of Δ and n_N are likely to occur as n_{up} is

increased into the detached regime. Conversely, bifurcation like behaviour must be expected when neutrals are confined to a reduced fraction of the connexion length, $L_N \ll L_{//}$, and/or when the effective control parameter is the neutral density n_N governed by the programmed gas injection. Finally, one must address the relationship between the n_{up} and $\langle n_e \rangle$. Results of the 1-D model, Fig. 2 plotted against the $\langle n_e \rangle$ are based on the following simplified expression.

$$\langle n_e \rangle = \alpha_{peak} n_{up} + \alpha_R |\Gamma_{div}| \frac{\lambda_I^{sep}}{D_\perp} \exp\left(- \frac{(\Delta_{div} - \Delta)}{\lambda_I^{div}} \right) + \alpha_{core} |\Gamma_{core}| \frac{\lambda_p}{D_\perp}. \quad (10)$$

The volume averaged density thus appears as a function of the boundary density, namely n_{up} with a prescribed peaking factor, α_{peak}, of the fuelling efficiency of the recycling particle flux in the divertor, and of direct core fuelling characterized by a penetration depth λ_p, and a particle flux Γ_{core}. In the ergodic divertor configuration, the latter fuelling is not used, $\alpha_{core} = 0$, so that feedback on the volume averaged density will determine the balance between the upstream density and direct core fuelling by the recycling flux. In the model, Fig. 2, $\alpha_{peak} \sim 3.5$ and direct core fuelling is only efficient during low density operation, typically the linear density regime, in agreement with the reported low fuelling efficiency of gas injection, typically 1% [6]. The screening factor of the recycling flux in Eq. (10) depends on the ratio of the active divertor volume $\Delta_{div} - \Delta$, where Δ_{div} is the extent of the low particle confinement region, to the ionization mean free path at the ionization front, λ_I^{div}. Following experimental observations [13], the fuelling efficiency increases as detachment occurs, hence as $\Delta_{div} - \Delta$ is reduced.

5. Conclusion

The comparison of the divertor density regimes in both the axisymmetric and ergodic divertor configurations demonstrates that similar physics govern the transition from linear to high recycling and from high recycling to detached regimes. Common features are a plasma state controlled by parallel transport associated to high particle screening leading to a large flux amplification in the divertor volume. It is shown that impurity radiation modifies the high recycling regime leading to a sharp increase of the divertor density, and, for a small increase of the volume averaged density, to divertor detachment below Greenwald density. Other common features which have been found are the effect of a reduction of the carbon source at high densities, in both helium and deuterium plasmas, which allows one to reach high densities with no detachment, i.e. no decrease of the electron pressure. In these deuterium shots, two plasma states are observed on flux tubes which exhibit large energy fluxes in the linear regime. Some flux tubes exhibit a sudden decrease of the divertor temperature following the model prediction of bifurcated states associated to the high recycling regime. In this case, the lowering of the carbon source leads to a state of nearly constant divertor temperature despite the increase of the volume averaged density. The other plasma state, so called 'death-ray' in C-Mod, is characterized by an increase of the divertor temperature prior to detachment.

The analysis of the location of the ionization front shows that open divertors, where plasma-neutral interaction is only bounded by the plasma, is characterized by a gradual detachment which is well characterized by a degree of detachment. Furthermore, these open configurations with large particle screening can be feedback controlled on the volume averaged density since the upstream plasma density can be increased in all regimes of density operation. Conversely, tight control of particle recirculation and in particular plasma baffling of neutrals in the private flux region or mechanical baffling of the neutrals in the divertor volume lead to an upper bound in the upstream density as long as baffling is efficient. Core density is then governed by direct core fuelling, i.e. no fuelling from the divertor as with strong NBI heating. These experiments are characterized by abrupt transitions to detachment when critical neutral densities are achieved. Present axisymmetric divertor experiments are working along this line to provide the experimental backing of the ITER divertor design. Given the significant hardware requirement to achieve mechanical baffling, these experiments cannot provide versatile configurations to estimate the benefit of tight control of particle recirculation. In this framework, the ergodic divertor offers a unique opportunity to operate an open divertor configuration with neutral baffling by the plasma itself.

Acknowledgements

The authors wish to thank the referees for their help in improving the paper.

References

[1] C.S. Pitcher, P.C. Stangeby, Plasma Phys. Contr. Fus. 39 (1997) 779.
[2] R. Schneider, Proc. Int. Conf. on Plasma Physics and Contr; Nucl. Fusion Research, Montreal 1996, vol. 2, International Atomic Energy Agency, Vienna, 1997, p. 465.
[3] M.L. Watkins, P.-H. Rebut, Proc. 19th Euro Conf. Plasma Physics and Contr. Fusion, vol. 16C, Innsbruck, European Physical Society, 1992, p. II-721.

[4] Ph. Chappuis and the Tore Supra team, J. Nucl. Mater. 241–243 (1997) 27.
[5] JET team presented by D. Stork, Proc. 16th Int. Conf. on Plasma Physics and Contr; Nucl. Fusion Research, Montreal 1996, vol. 1, International Atomic Energy Agency, Vienna, 1997, p. 189.
[6] Ph. Ghendrih, A. Grosman, H. Capes, Plasma Phys. Contr. Fus. 38 (1996) 1653.
[7] Y. Sarazin, Ph. Ghendrih, X. Garbet, Proc. 24th Euro Conf. on Plasma Physics and Contr. Fusion, vol. 21A, Berchtesgaden, European Physical Society, 1997, p. I-193.
[8] S. Féron, PhD thesis, Transport de la chaleur dans un champ magnétique chaotique, 1997, Report EUR-CEA-FC-1616, December 1997.
[9] B. LaBombard, J.A. Goetz, I. Hutchinson et al., J. Nucl. Mater. 241–243 (1997) 49.
[10] B. Meslin, T. Loarer, Ph. Ghendrih, A. Grosman, these Proceedings.
[11] P. Monier-Garbet, C. DeMichelis, Ph. Ghendrih et al., these Proceedings.
[12] H. Capes, Ph. Ghendrih, A. Samain, Phys. Fluids B 4 (1992) 1287.
[13] C. Grisolia, Ph. Ghendrih, A. Grosman, P. Monier-Garbet, D. Moulin, J.-C. Vallet, Feedback control of high radiative plasmas in Tore Supra, presented at 13th Int. Conf. on Plasma–Surface Interaction in Controlled Fusion Devices (PSI-13), San Diego, CA, May 1998.
[14] A. Loarte, Nucl. Fusion 38 (1998) 331.
[15] Tore Supra team presented by Ph. Ghendrih, Plasma Phys. Contr. Fusion 39 (1997) B207.
[16] C. DeMichelis, Ph. Ghendrih, R. Guirlet et al., Plasma Phys. Contr. Fusion 37 (1995) 505.
[17] N. Hosogane, N. Asakura, H. Kubo et al., J. Nucl. Mater. 196–198 (1992) 750.
[18] M.E. Fenstermacher, R.D. Wood, S.L. Allen et al., J. Nucl. Mater. 241–243 (1997) 666.
[19] B. Lipschultz, J. Goetz, B. LaBombard et al., J. Nucl. Mater. 220–222 (1995) 50.
[20] D.N. Hill, and the DIII–D Divertor Group, Divertor detachment in DIII–D helium plasmas, Phys. Plasmas, to be published.
[21] P. Stangeby, in: D.E. Post, R. Behrisch (Eds.), Physics of Plasma-Wall Interactions in Controlled Fusion, vol. 131, Nato ASI series, series B, Plenum, NY, 1986, p. 41.
[22] Ph. Ghendrih, Phys. Plasmas 1 (1994) 1929.
[23] Ph. Ghendrih, H. Capes, Proc. 15th Int. Conf. on Plasma Physics and Contr.; Nucl. Fusion Research, vol. 3, Sevilla 1994, International Atomic Energy Agency, Vienna, 1996, p. 441.
[24] I.H. Hutchinson, Phys. Fluids 30 (1987) 3777.
[25] J.P. Gunn, Ph. Ghendrih, A. Grosman, B. Meslin, J.Y. Pascal, Measurements of the ion speed in Tore Supra Ergodic Divertor experiments, 25th EPS, Praha, June 1998, to be submitted.
[26] Ph. Ghendrih, T.W. Petrie, C. Lasnier et al., J. Nucl. Mater. 220–222 (1995) 305.
[27] T.W. Petrie, D. Buchenauer, D.N. Hill et al., J. Nucl. Mater. 196–198 (1992) 842.